Research Article
Experimental and Translational Hepatology

JOURNAL
OF HEPATOLOGY

Interferon-induced IL-10 drives systemic T-cell dysfunction during chronic liver injury

Authors

Carl-Philipp Hackstein, **Jasper Spitzer**, Konstantinos Symeonidis, …, Susanne V. Schmidt, Percy A. Knolle, Zeinab Abdullah

Correspondence

zeinab.abdullah@uni-bonn.de (Z. Abdullah).

Graphical abstract

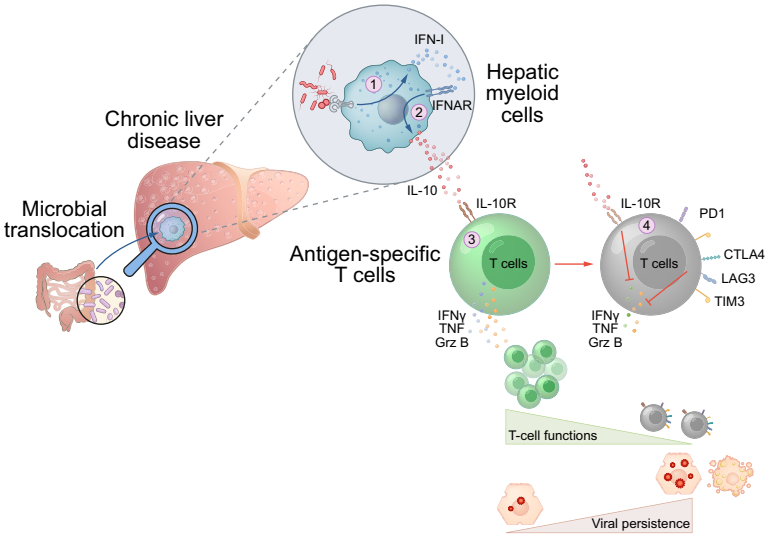

Highlights

- During chronic liver injury, antigen-specific T cells feature hallmarks of T-cell exhaustion.
- IFN-I/IL-10 signaling axis is a determinant of impaired systemic T-cell responses in chronic liver injury and cirrhosis.
- IFN-I-induced by translocated gut microbiota hampers systemic T-cell immunity *via* IL-10 release by myeloid cells.
- IL-10 suppresses T-cell immunity by directly acting on antigen-specific T cells.
- IL-10R blockade promotes the reconstitution of T-cell functions in virus infected mice and vaccinated patients.

Impact and implications

Chronic liver injury and cirrhosis are associated with enhanced susceptibility to viral infections and vaccine hyporesponsiveness. Using different preclinical animal models and patient samples, we identified that impaired T-cell immunity in BDL- and CCL_4-induced prolonged liver injury is driven by sequential events involving microbial translocation, IFN signaling leading to myeloid cell-induced IL-10 expression, and IL-10 signaling in antigen-specific T cells. Given the absence of immune pathology after interference with IL-10R, our study highlights a potential novel target to reconstitute T-cell immunity in patients with CLD that can be explored in future clinical studies.

https://doi.org/10.1016/j.jhep.2023.02.026
 J. Hepatol. 2023, 79, 150–166

Research Article
Experimental and Translational Hepatology

JOURNAL
OF HEPATOLOGY

Interferon-induced IL-10 drives systemic T-cell dysfunction during chronic liver injury

Carl-Philipp Hackstein[1,12,‡,†], **Jasper Spitzer**[2,‡,†], Konstantinos Symeonidis[1], Helena Horvatic[1], Tanja Bedke[3], Babett Steglich[3], Sabine Klein[4], Lisa M. Assmus[1], Alexandru Odainic[2], Jennifer Szlapa[1], Nina Kessler[1], Marc Beyer[5], Ricarda Schmithausen[6], Eicke Latz[2], Richard A. Flavell[7], Natalio Garbi[1], Christian Kurts[1], Beate M. Kümmerer[8,9], Jonel Trebicka[4], Axel Roers[10], Samuel Huber[3], Susanne V. Schmidt[2], Percy A. Knolle[11,13,‡], Zeinab Abdullah[1,*,‡]

Journal of Hepatology **2023**. vol. 79 | 150–166

Check for updates

Background & Aims: Patients with chronic liver disease (CLD), including cirrhosis, are at increased risk of intractable viral infections and are hyporesponsive to vaccination. Hallmarks of CLD and cirrhosis include microbial translocation and elevated levels of type I interferon (IFN–I). We aimed to investigate the relevance of microbiota-induced IFN-I in the impaired adaptive immune responses observed in CLD.

Methods: We combined bile duct ligation (BDL) and carbon tetrachloride (CCl_4) models of liver injury with vaccination or lymphocytic choriomeningitis virus infection in transgenic mice lacking IFN-I in myeloid cells (LysM-Cre IFNAR$^{flox/flox}$), IFNAR-induced IL-10 (MX1-Cre IL10$^{flox/flox}$) or IL-10R in T cells (CD4-DN IL-10R). Key pathways were blocked *in vivo* with specific antibodies (anti-IFNAR and anti-IL10R). We assessed T-cell responses and antibody titers after HBV and SARS-CoV-2 vaccinations in patients with CLD and healthy individuals in a proof-of-concept clinical study.

Results: We demonstrate that BDL- and CCL_4-induced prolonged liver injury leads to impaired T-cell responses to vaccination and viral infection in mice, subsequently leading to persistent infection. We observed a similarly defective T-cell response to vaccination in patients with cirrhosis. Innate sensing of translocated gut microbiota induced IFN-I signaling in hepatic myeloid cells that triggered excessive IL-10 production upon viral infection. IL-10R signaling in antigen-specific T cells rendered them dysfunctional. Antibiotic treatment and inhibition of IFNAR or IL-10Ra restored antiviral immunity without detectable immune pathology in mice. Notably, IL-10Ra blockade restored the functional phenotype of T cells from vaccinated patients with cirrhosis.

Conclusion: Innate sensing of translocated microbiota induces IFN-/IL-10 expression, which drives the loss of systemic T-cell immunity during prolonged liver injury.

Introduction

Chronic liver diseases (CLD) such as liver fibrosis and cirrhosis are associated with barrier dysfunction and enhanced microbial translocation into the liver, leading to tonic and chronic type I interferon (IFN–I) signaling, release of pro-inflammatory cytokines and chronic immune cell activation.[1,2] As the disease progresses, systemic inflammation and structural distortion of liver tissue are believed to determine progressive loss of immune surveillance known as cirrhosis-associated immune dysfunction (CAID).[3] Enhanced susceptibility to infections[4–6] and poor response to vaccination against influenza, hepatitis A and hepatitis B constitute major factors contributing to patient's morbidity and mortality.[3,7–9] We have previously shown that IFN-I acting on hepatic myeloid cells in the context of bacterial infection during liver damage is responsible for impaired innate immunity in mouse and man.[1] Interestingly, excessive IFN-I signaling has also been shown to be involved in loss of T-cell functionality in chronic viral infections,[10] rendering the immune system unable to contain infection.

Herein, we report that tonic IFN-I signaling during prolonged liver injury (hereafter referred to as pLI) and cirrhosis determines the loss of systemic CD8 and CD4 T-cell-mediated immunity through induction of the immune-regulatory cytokine IL-10. In preclinical models of bile duct ligation (BDL)- and carbon tetrachloride (CCL_4)-induced pLI and patients with cirrhosis, we identified IL-10 as the key mediator of T-cell dysfunction during chronic liver injury and provide evidence that blocking IL-10 rescues T-cell function and allows for control of viral infection without immune pathology in mice. Given the importance of CD8 and CD4 T-cell responses for immune surveillance, our findings contribute to the understanding of failing immune

Keywords: Chronic liver disease; fibrosis; cirrhosis; T-cell immunity; viral infection; vaccination.
Received 10 August 2022; received in revised form 8 February 2023; accepted 13 February 2023; available online 2 March 2023
* Corresponding author. Address: Venusberg Campus 1, University Hospital Bonn, 53127 Bonn, Germany; Tel.: +49 228 287 11138, fax: +49 228 287 51204.
E-mail address: zeinab.abdullah@uni-bonn.de (Z. Abdullah).
† Contributed equally as first authors
‡ These authors contribute equally
https://doi.org/10.1016/j.jhep.2023.02.026

responses in patients with cirrhosis and identify the IL-10Ra signaling pathway as a potential molecular target to improve immune control and vaccination efficacy in these patients.

Materials and methods

Patients and blood samples

Blood and serum samples as well as questionnaire-based assessment of donor characteristics and disease stage were collected from patients with cirrhosis and healthy volunteers before vaccination with TWINRIX (HAV and HBsAg) at the University Hospital Bonn and general practices in Bonn (healthy individuals, n = 16; patients with cirrhosis, n = 16). All enrolled participants had never been exposed to HBV or vaccinated against HBV or HAV, as proven by the absence of anti-HBs antibodies on serological testing before vaccination. Informed consent was obtained from all patients and healthy individuals enrolled in the trial in accordance with the Declaration of Helsinki protocol. The study was approved by and performed according to the guidelines of the local ethics committees of the University of Bonn (310/16). All enrolled participants received four doses of the vaccine on day 1, 7, 21 and after 6 months. Sample collection was performed 4 to 5 weeks after the last injection. Peripheral blood mononuclear cells (PBMCs) were isolated by Ficoll-Hypaque (PromoCell, Germany) density gradient centrifugation and stored at –80 °C until further use. Serum was separated by centrifugation for 10 min and supernatant was stored at –80 °C. Detailed characteristics of healthy donors and patients with CLD and the study design are provided in Table S1 and S2 and Fig. S1E,F.

HBs-specific T-cell activation

Forty-three (80-90% purity) 15-mer synthetic peptides, overlapping by 10 amino acids (Xaia Custom Peptides, Sweden) and covering the sequence of the HBV surface antigen (HBsAg) protein according to the Galibert sequence, were generated (Table S3). Peptides were pooled and used for detection of HBs-specific T cells and their function. After isolation from peripheral blood, untouched CD3 T cells were labelled with CellTrace Violet (0.5 μM; Thermo Fisher Scientific) and cultured in round-bottom 96-well plates at 5×10^4/well, in the presence of autologous irradiated (4,000 rads) PBMCs (10^5/well), HBs peptides and recombinant human IL-2 (50 U/ml; PeproTech). After 5 days of incubation, proliferation and cytokine production in HBs-specific T cells were assessed by flow cytometry.

Anti-RBD (S) SARS-CoV-2 antibodies assay

Serum samples were analyzed for anti-S-RBD IgG titers using the SARS-CoV-2 Plate 7 V-PLEX Serology Kit from MSD (Meso Scale Diagnostics, LLC). Antibody concentrations were quantified via the MESO SECTOR S 600. Raw data was analyzed with the MSD Discovery Workbench tool (V 4.0.13), that quantifies anti-RBD IgG. All assays were performed by trained laboratory technicians according to the manufacturer's standard procedures.

SARS-CoV-2 neutralization assay

Heat-inactivated sera were serially twofold diluted starting with 1:5 dilutions. 120 μl of each serum dilution was mixed with 120 μl of OptiPRO™ SFM cell culture media (Gibco) containing 80 plaque-forming units (PFUs) of SARS-CoV-2 (isolate B.3). After 1 h at 37 °C, 200 μl of each mixture was added to wells of a 24 well plate seeded the day before with $1.5 \times 10e^5$ Vero E6 cells/well. After incubation at 37 °C for 1 h, the inoculum was removed and cells were overlaid with a 1:1 mixture of 1.5% carboxymethylcellulose (Sigma) in 2x MEM (Biochrom) with 4% FBS (Gibco). After a 3-day incubation at 37 °C, cells were fixed with 6% formaldehyde and stained with 1% crystal violet in 20% ethanol.

In vitro activation and proliferation assay of human T cells

PBMCs were labelled with CellTrace Violet (0.5 μM; Thermo Fisher Scientific) and cultured in RPMI supplemented with 10% FCS at 1×10^6 cells/well in 96-well plates (Corning) coated with anti-CD3 (clone HIT3a, BioLegend), anti-CD28 (clone L293, BD Biosciences) (each at 3 μl/ml) and IL-2 (10 IU/ml; PeproTech). T-cell proliferation and intracellular cytokine expression, as well mitochondrial assays, were assessed by flow cytometry.

In vitro IL-10Ra blockade on human T cells

PBMCs were cultured in RPMI supplemented with 10% FCS at 1×10^6 cells/well in 96-well plates (Corning) coated with anti-CD3 (clone HIT3a, BioLegend) and anti-CD28 (clone L293, BD Biosciences) (each at 3 μl/ml) and IL-2 (10 IU/ml; PeproTech). 5 μg/ml of the blocking anti-IL-10Ra antibody (3F9; BioLegend) was added 12 h later.

ELISA for detection of cytokine expression

Human IFNg, TNF and IL-2 in the supernatant of *in vitro*-activated cells and murine IL-10 in the serum were detected using ELISA MAX Deluxe Set (BioLegend) according to the manufacturer's instructions.

Quantification of mitochondrial membrane potential, mitochondrial mass and mitochondrial superoxide production

Mitochondrial studies in human T cells were performed after anti-CD3 stimulation. Cells were incubated with 50 nM MitoTracker Green (MTG) and/or 25 nM MitoTracker DeepRed (MTDR) for 30 min at 37 °C before cell surface staining. Mitochondrial superoxide levels in human T cells were determined, after cell surface staining, by incubation (15 min at 37 °C) of overnight anti-CD3 stimulated and unstimulated cells in the presence of MitoSOX Red (5 μM; Molecular Probes).

Mice

6–9-week-old mice C57BL/6J (B6) were purchased from Janvier (Le Genest-Saint-Isle, France. $LysM^{Cre}$-$IFNAR^{fl/fl}$ (previously described[18]), OT-I, OT-II, CD45.1-B6 (B6.SJL-Ptprca Pepcb/BoyJ), 6C2.36 and P14 mice were originally purchased from The Jackson Laboratory and maintained in the House of Experimental Therapy, University Clinic Bonn. $Mx1^{Cre}$-$Il10^{fl/fl}$ x $Mx1^{Cre}$ ($(Il10^{tm1Roer})$ x (C.Cg-Tg(Mx1-Cre)1Cgn/J)) were kindly provided by Axel Roers. $IL10Ra^{DN}$ mice[43] were kindly provided by Samuel Huber. All mice were maintained under specific pathogen-free (SPF) conditions and were handled according to the guidelines of the institutional animal guidelines of the animal

facilities of the University of Bonn. Experimental procedures were approved by the Animal Ethics Committee of the state of North Rhine-Westphalia, Germany. For antibiotic treatment, mice were given a combination of vancomycin (1 g/L), ampicillin (1 g/L), kanamycin (1 g/L), and metronidazole (1 g/L) in drinking water[72]. All antibiotics were obtained from Sigma Aldrich. Colonization of germ-free (GF) mice with caecal microbiota of SPF mice was performed as previously described[73]. Briefly GF mice received a suspension of the cecum content from wild-type (WT) mice (who had undergone a sham operation or BDL) by oral gavage on 3 consecutive days, and underwent BDL 1 week after the last transfer.

Murine liver injury models

Liver injury was induced in 8–9-week-old male mice via BDL or treatment with CCl_4 following established protocols[75]. In brief, to induce BDL, the animals were treated with painkillers and anaesthetized before the peritoneal cavity was opened along the *linea alba*. Two ligatures were placed around the common bile duct in order to obstruct it, the incisions in the peritoneum and the skin were then closed and the mice were allowed to recover. During the first 5 days after the operation all animals received additional injections of painkillers and liver injury was allowed to develop for 10 days before experiments were performed. Alternatively, mice received 0.5 μl CCl_4/g body weight for 12 weeks intraperitoneally. CCl_4 was dissolved 1:7 in olive oil and was administered at 3-day intervals. After the final injection, mice were allowed to recover for 10 days before further experiments were performed. Control mice underwent a sham operation (no ligation of the bile duct) or received olive oil (i.p.) injections respectively. During all experiments, animals were monitored closely on a daily basis. To inhibit the IFN alpha receptor (IFNAR) or interleukin 10 receptor-alpha (IL-10Ra) signaling *in vivo*, mice were treated intraperitoneally with 250 μg/mouse of blocking antibodies targeting TGFBR-II (clone: 1D11.16.8), IFNAR1 (clone: MAR1-5A3), or IL-10Ra (clone: 1B1.3A) from BioXcell. Control animals received injections containing the HPRN and MOPC-21 antibodies respectively.

LCMV infection

Mice were infected with $2x10^4$ PFUs of lymphocytic choriomeningitis virus (LCMV) strain WE or Armstrong diluted in sterile PBS intravenously.

Irradiation and adoptive cell transfers

Mice were subjected to sublethal irradiation (6 Gy) one day before transfer. T cells were isolated from the spleens and lymph nodes of donor mice and $4x10^6$ $CD3^+$ T cells (1:1 of WT and transgenic [TG] cells) per recipient were transferred intravenously. Before any subsequent experiment, recipient mice were allowed to recover for 12 days in order to ensure proper engraftment. For all other infection or vaccination studies, Naïve P14, OT-I and OT-II cells were isolated from the spleens of mice and $2.5x10^5$ cells were transferred 1 day before vaccination.

Murine in vitro T-cell proliferation assay

48-well plates were coated with antibodies directed against murine CD3 (clone: 500A.2, BD Biosciences) and CD28 (clone: 37.51, Biolegend) at a concentration of 0.5 μg/ml and 10 μg/ml, respectively, incubated at 37 °C for 2 h and washed. T cells isolated from the spleens of sham-operated or BDL mice were stained with CellTrace Violet (Thermo Fisher Scientific) and added at a concentration of $2x10^6$ cells/ml. T-cell proliferation was measured after 3 days by flow cytometry.

Flow cytometry and antibodies

Single-cell suspensions were acquired on a FACSCanto II or LSRII Fortessa (DFG ID 216372401) and analyzed with FlowJo (version 10.0.7, Tree star). In order to determine the expression of surface molecules, cells were stained on ice for 20 min. The LIVE/DEAD fixable Near-IR Dead Cell Stain kit (Life Technologies) was used in all staining to detect dead cells, also, an in-house antibody (clone: 2.4G2) directed against the epitopes shared by Fc-gamma receptors was added. Single-cell suspensions from spleen or liver were stimulated with 100 ng/ml or 200 ng/ml PMA, in the presence of Brefeldin A and monensin for 3 h, before collection and intracellular staining for flow cytometry. To block unspecific staining, cytokines were stained after fixation with 4% PFA and permeabilization with 1x Permeabilization buffer (FoxP3/Transcription Factor Staining Buffer Set, eBioScience) and transcription factors with the FoxP3/Transcription Factor Staining Buffer Set according to the manufacturer's instructions. Antibodies directed against the following targets in mice were purchased from Biolegend, eBioScience or Miltentyi: anti-CD3e (145-2C11), anti-CD4 (GK1.5 or RM4-5), anti-CD8a (53-6.7), anti-CD11b (M1/70), anti-CD11c (N418), anti-CD44 (1M7), anti-CD45.1(A20), anti-CD45.2(104), anti-CD146 (ME-9F1), anti-CD210a (1B1.3a), anti-CTLA-4 (UC10–4B9), anti-Eomes (Dan11mag), anti-F4/80 (BM8), anti-GzmB (GB11), anti-IFNg (XMG1.2), anti-IL-2 (JES6-5H4), anti-IL-21 (FFA2), anti-LAG3 (C9B7W), anti- PD-1 (29F.1A12), anti-T-bet (4B10), anti-IRF4 (IRF4.3E4), anti-TOX (TXRX10), anti-TCF-1 (S33-966), anti-TCRb (H57.597), anti-TIM3 (RMT3-23) and anti-TNF (MP6-XT22), anti-phospho-STAT3 (Stat3Y705–B12) and anti-phospho-SMAD2 (Ser250 (SD207-1)). CD8 and CD4 T-cell tetramers specific for the LCMV epitopes gp33-41 and gp66-77, respectively, were purchased from Immudex (gp33-dextramer) or provided by the NIH Tetramer Core Facility (Emory University). The following antibodies were used to detect protein expression on human cells: anti-CD3 (SK3), anti-CD62L (DREG-56), anti-CD8 (PRA-T8), anti-CD45RA (HI100), anti-CD45 (HI30) from ThermoFisher, and anti-CD4 (PRA-T4), anti-PD1 (EH12.2H7), anti-CTLA4 (BNI3), anti-CD3 (OKT3), anti-IFNg (4S.B3), anti-IL-21 (3A3-N2), anti-IL-10Ra (3F9) from BioLegend.

Immunofluorescence microscopy

Liver tissue samples were fixed in a 0.05 M phosphate buffer containing, 0.1 M L-lysine, 2 mg/ml $NaIO_4$, and 10 mg/ml paraformaldehyde at pH7.4 overnight. Subsequently, samples were washed in phosphate buffer and dehydrated in 30% sucrose overnight. Finally, samples were place in Tissue TEK (Sakura Finetek), snap-frozen and stored at -80 °C. 20 μm sections were acquired on a CM3050S cryostat, rehydrated and stained with antibodies in buffer containing 1% normal mouse serum. Pictures were acquired on an LSM 710 confocal Microscope (Zeiss). A BV421-conjugated antibody directed against F4/80 (BM8) was purchased from Biolegend; for detection of the LCMV nucleoprotein, an unconjugated rat-anti-

LCMV antibody (VL4) was purchased from BioXCell; expression was detected via an AF647-conjugated goat-anti-rat antibody (Invitrogen).

RNA extraction, cDNA-synthesis and RT-PCR

Small samples of liver tissue were homogenized in 1 ml Quiazol and total RNA was isolated using the RNeasy Lipid Tissue Kit (Quiagen, 74804). Afterwards, 2-5 μg of RNA was reverse transcribed into cDNA at 37 °C for 2 h using the High-Capacity cDNA Reverse Transcription Kit (Applied Biosystems, 4368814). cDNA was stored at -20 °C and real-time PCR was performed using Taqman primers and probes for *Il10*, *Ifnb1*, *Mx1*, *Hprt* and *Gapdh* in murine samples and *PDCD1*, *CTLA4*, *CD244*, *EOMES*, *BATF*, *GAPDH* and *HPRT* in human samples. The relative mRNA expression was calculated with the ΔΔCt-method.

RNA sequencing and data analysis

Transcriptomic differences in isolated T cells from BDL or sham-operated mice were determined by QuantSeq 3'mRNA sequencing (Lexogen). FACS (Aria Fusion DFG ID 387333827) sorted cells were lysed in 700 μl Trizol and stored until RNA extraction was performed with the RNeasy micro kit (Qiagen). Library production for 3'-mRNA sequencing was performed with up to 160 ng purified RNA according to the manufacturers' protocol and sequenced on a HiSeq2500 (Illumina) with a sequencing depth of 15 Mio reads per sample (NGS Core Facility, University Hospital, Bonn, Germany). The alignment was performed with STAR (v2.5.3a) against the murine reference genome mm10. Transcripts were quantified with the Partek E/M algorithm and further processed for normalization in R (v3.5.0) with the DEseq2 algorithm (v1.20.0). The data set was further optimized by flooring transcripts with minimal gene counts at least to ≤1 and the exclusion of transcripts with a mean expression ≤10 in every test condition. Differentially expressed genes were identified in the Partek Genomics Suite (v7.18.0402) for T cells isolated from BDL *vs*. sham-operated mice using a one-way-ANOVA (fold-change |1.5|, false discovery rate-adjusted *p* value ≤0.05). Data visualization and biological interpretation were performed with the Partek Genomics Suite, ClueGo plugin (v2.5.2) for Cytoscape (v3.7.2) and R packages ggplot2 (v3.2.1), Enhanced Volcano (v1.6) and tidyr (v1.0.2). Heatmaps of two groups were created using means across the two groups, with expression being centered around 0 and visualized with Mayda (v2.14).

16S qPCR for quantification of bacterial DNA

DNA was extracted from samples using MoBio PowerSoil kit (Qiagen). DNA concentration was calculated using a standard curve of known DNA concentrations from *E. coli* K12. 16S qPCR with primers identifying different regions of the V6 16S gene was performed using Kappa SYBR fast mix. The absolute number of bacteria in the samples was then approximated as DNA amount in a sample/DNA molecule mass of bacteria. Liver tissue of GF mice was used as an internal control.

Statistical analysis

To determine statistical differences, a two-tailed unpaired or paired Student's *t* test was used when two groups were compared; a repeated-measurements one-way ANOVA was used when three groups were compared. For non-parametric data, the Mann-Whitney test was used when comparing two groups and the Kruskal-Wallis test when comparing three or more groups, respectively. Analysis was performed with Prism 8. Statistical significance was set at $p < 0.05$.

Results

Failure of T-cell immunity to control viral infection in mice with CLD

To explore the impact of CLD on T cell-mediated antiviral immune responses, we combined two different mouse models of pLI (*i.e.*, BDL and CCl_4 treatment) with LCMV-WE and LCMV-Armstrong strain infections, which are rapidly cleared by the T-cell response in healthy mice. While healthy mice successfully controlled LCVM replication by day 12 at the latest (Fig. 1A-C, Fig. S1A-D, data not shown), BDL and CCl_4-treated mice failed to clear LCMV-WE from blood, liver and spleen and viral replication persisted for at least 30 days post infection (p.i.), indicating a systemic loss of antiviral immune surveillance, rather than a local attenuation of antiviral immunity selectively in the liver. At the peak of the immune response, *i.e.* day 8 p.i., pLI mice showed significantly lower numbers of LCMV-specific CD8 T cells recognizing the gp33 epitope of LCMV compared to healthy mice (Fig. 1D,E and Fig. S1E,F). Moreover, fewer LCMV-specific CD8 T cells were present (and a lower percentage were IFNg/TNF-producing) in pLI mice (Fig.1F,G, Fig. S1G), indicating loss of antiviral immune surveillance during pLI independent of its aetiology. Of note, we observed reduced numbers of LCMV-specific CD4 T cells in BDL mice (Fig. 1H,I), that had diminished effector cytokine production with only few cells co-expressing IFNg, TNF and IL-2 (Fig. S1H,I). To study the defect in virus-specific CD8 T cells in more detail, we transferred TCR-TG P14 CD8 T cells, which express a T-cell receptor specific for the LCMV-gp33 epitope, into BDL mice 1 day before LCMV infection. BDL mice showed reduced frequencies and numbers of IFNg/TNF-producing T cells compared to sham mice (Fig. S1J-M), confirming the results observed in endogenous T cells. Together, these experiments demonstrated a broad and severe dysfunction of virus-specific T-cell immunity in pLI mice that was associated with failure to control LCMV infection.

Defective T-cell responses to vaccination in patients and mice with liver injury

To assess whether the observations made in the mouse models of BDL- and CCL_4-induced prolonged liver injury recapitulate the phenotype of T cells from patients, we stimulated PBMC-derived T cells from healthy individuals and patients with cirrhosis (Table S1) with anti-CD3/CD28 antibodies to induce antigen-mediated T-cell activation. T cells from patients with CLD produced significantly lower levels of IL-2, IFNg and TNF (Fig. 2A) which were associated with enhanced apoptosis ($AnnexinV^{positive}$), lower mitochondrial membrane potential, higher numbers of depolarized mitochondria, and higher levels of reactive oxygen species that failed to increase upon stimulation (Fig. S2A-D). To explore the mechanisms of CLD-associated T-cell dysfunction, we studied the responses of patients with cirrhosis and healthy individuals (Table S1) to

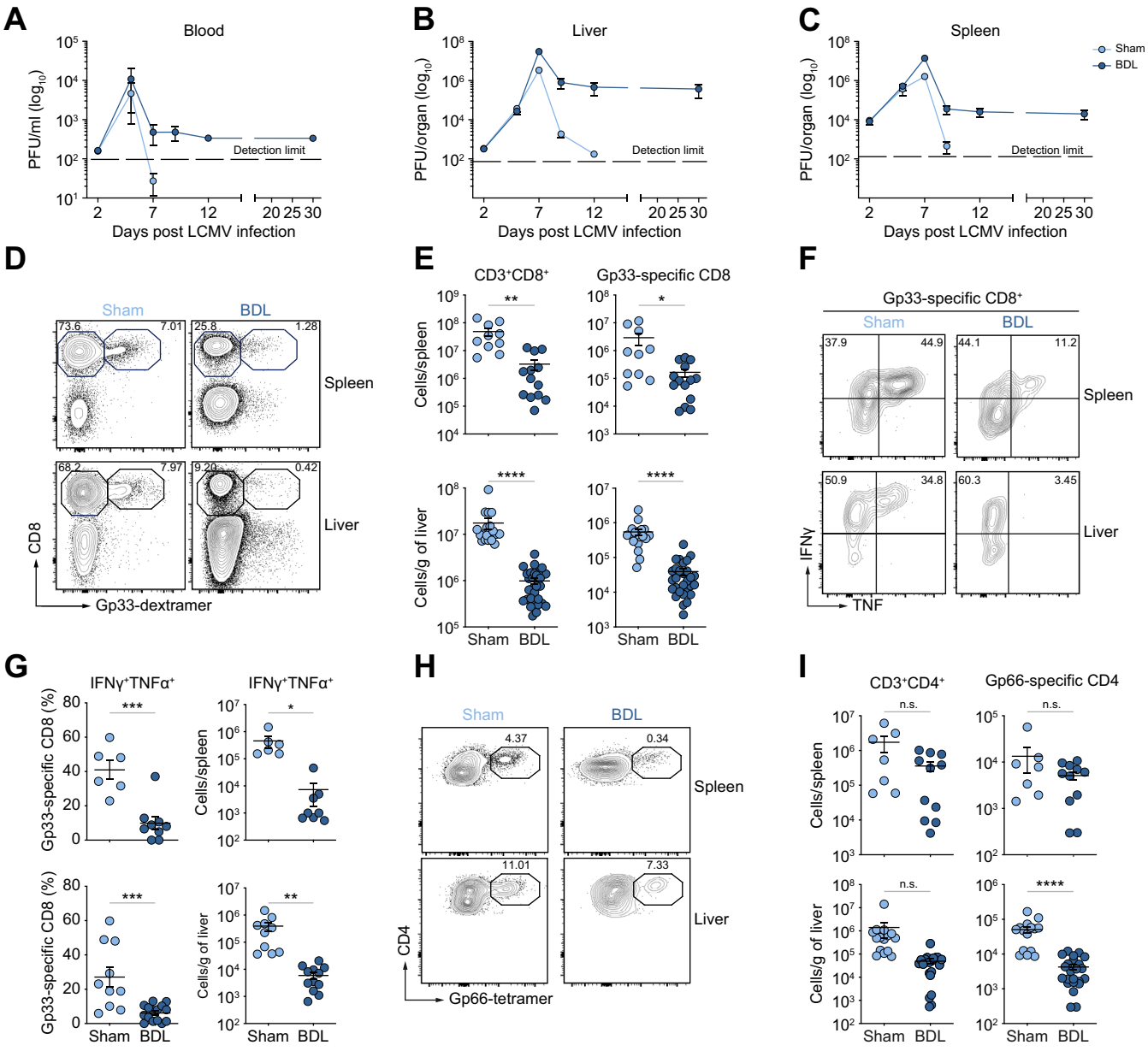

Fig. 1. Impaired antiviral T-cell responses in mice with pLI. BDL- or sham-operated mice were infected with LCMV (2×10^4 PFU) on day 9 post-operation. (A-C) LCMV titers (PFU) in the blood, liver and spleen. (D,E) Total and gp33-specific CD8 T cells from spleen and liver on day 8. (F,G) IFNg/TNF production by LCMV-specific CD8 T cells. (H,I) Frequencies of total and LCMV-specific CD4 T cells on day 8. (A-C) Data representative of ≥3 independent experiments; (E,G,I) pooled data from ≥3 independent experiments; statistical analysis by unpaired *t* test. BDL, bile duct ligation; gp33, glycoprotein 33; PFU, plaque forming unit.

HBV vaccination in a proof-of-concept clinical study (Fig. S2E). In line with previous studies,[11] 94% of the healthy vaccinees had anti-HBs antibody titers >100 IU/L (strong responders) after vaccination, while only 38% of patients with cirrhosis had a titer >100U/L, and 62% had titers between 10-100 IU/L (weak responders) (Fig. 2B). Furthermore, HBs-specific blood-derived CD8 and CD4 T cells from patients with cirrhosis failed to proliferate and to produce IFNg and IL-21 after stimulation with HBs-specific peptides (Fig. 2C-F). Additionally, we assessed the response to SARS-CoV-2 vaccination in naïve patients with cirrhosis and healthy individuals (Table S2) who received two doses of mRNA (BNT162b2) vaccine (Fig. S2F). Blood samples were obtained before and 7-10 days after the second vaccination. RBD IgG binding to WT virus – as well as variants of concern, such as B1.351 (beta), B.1.1.7(alpha) and P.1(gamma) – and neutralization capacity were significantly lower in patients with cirrhosis compared to healthy individuals (Fig. 2G,H, Fig. S2G). Likewise, CD4 and CD8 T cells from patients with cirrhosis produced significantly lower levels of IFNg upon *in vitro* stimulation with spike protein peptides (Fig. 2I). Together, these results indicate impaired antigen-specific B- and T-cell immunity after vaccination in patients with cirrhosis.

To characterize impaired T-cell immunity after vaccination *in vivo*, we transferred naïve HBs-specific (6C2.36) or ovalbumin-specific CD45.1$^+$CD8 (OT-I) and CD4 (OT-II) TG T

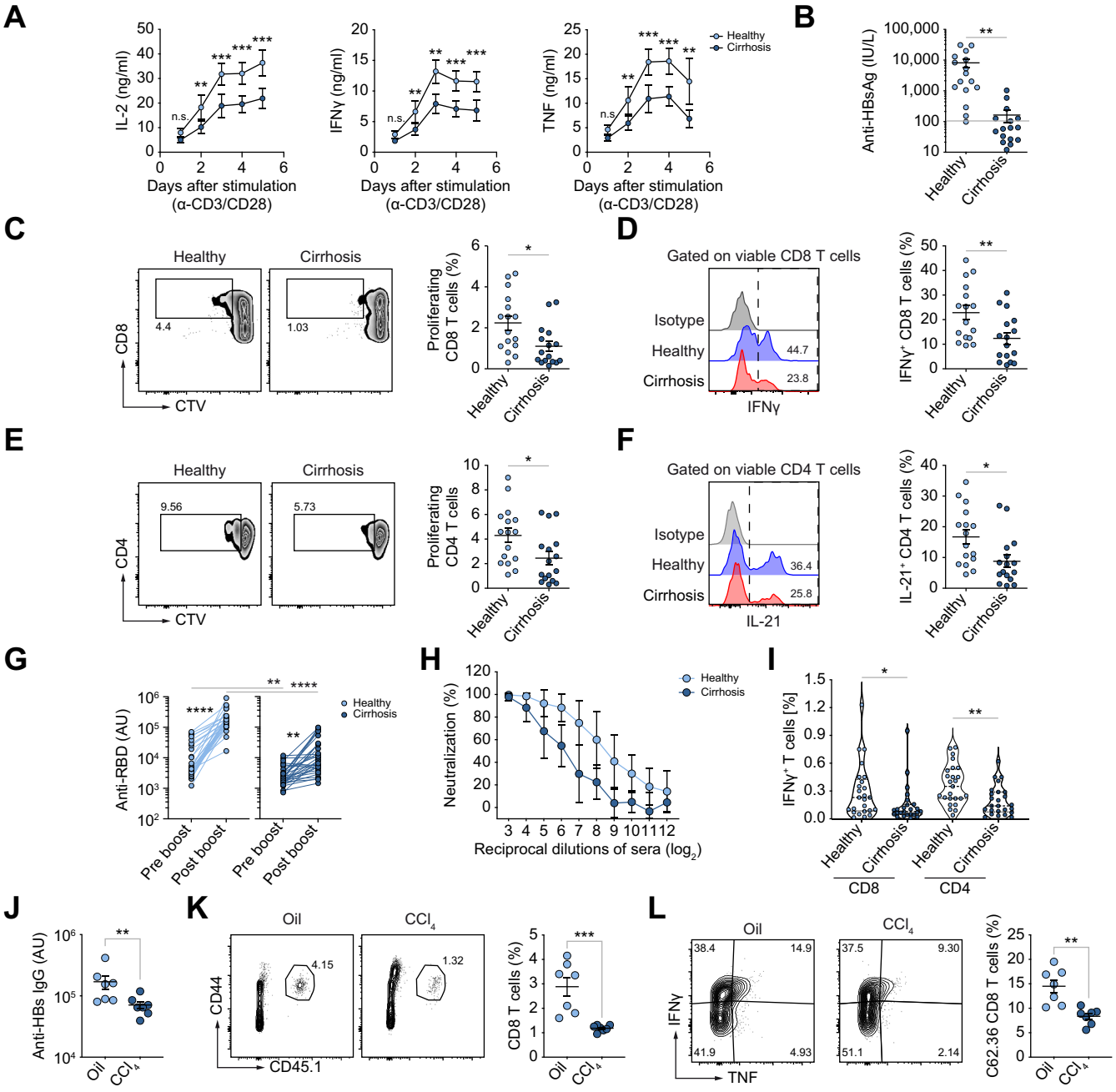

Fig. 2. Poor immune responses to vaccination in patients and mice with cirrhosis. (A) IL-2, IFNg/TNF-release from anti-CD3/CD28-stimulated T cells from healthy donors or patients with cirrhosis. (B) anti-HBs IgG titers in the sera of healthy donors (n = 16) and patients with cirrhosis (n=16) vaccinated against HBs Ag. (C–F) Frequencies of proliferating and IFNg-producing CD8 T cells or IL-21-producing CD4 T cells after *ex vivo* stimulation with HBsAg peptides. (G) Serum IgG binding to RBD of SARS-CoV-2 at day 7-10 after the second SARS-CoV-2 mRNA vaccination (BNT162b2). (H) Neutralization of wild-type SARS-CoV-2 by the sera of healthy (n = 7) or cirrhosis (n = 9) vaccinees.(I) Frequencies of IFNg-producing CD8 and CD4 T cells after *in vitro* stimulation with SARS-CoV-2 spike protein. (J-L) Oil- or CCl_4-treated (12 weeks) mice were vaccinated with HBsAg/polyI:C. (J) Anti-HBs IgG titer on day 7. (K) Percentages of splenic CD45.1+ HBs-specific (6C2.36) CD8 T cells. (l) Frequency of IFNg/TNF-producing CD8 T cells. Data representative of three (A) or two (H,J,K,L) independent experiments. (A-F, I-L) Statistical analysis by unpaired *t* test, (G) paired Wilcoxon. BNT, Pfizer BioNTech; CCl_4, carbone tetrachloride; HBsAg, hepatitis B virus surface antigen; RBD, receptor binding domain.

cells into CCl_4-treated and BDL mice, respectively, 1 day before vaccination with HBs antigen or ovalbumin with polyI:C as an adjuvant. In line with the results from patients with CLD, we detected significantly lower titers of anti-HBs antibodies (Fig. 2J) as well as lower frequencies of 6C2.36 (Fig.2k,l), and lower frequencies of OT-I and OT-II cells and reduced frequencies of IFNg-, TNF- and IL-2- producing specific T cells (Fig. S2H-K) in the spleen of pLI mice, which suggest reduced T-cell expansion and effector function. Together, these findings suggest that systemic antigen-specific T-cell responses to vaccination were impaired during chronic liver disease and cirrhosis.

Liver injury renders virus-specific T cells dysfunctional

To fine-map the transcriptional profile of antigen-specific CD8 T cells during pLI, we performed bulk RNA-seq analysis of sorted P14 cells from BDL or sham-operated mice at day 8 post LCMV infection and identified 2,153 differentially expressed genes (Fig. S3A). Gene ontology enrichment analysis and network visualization revealed differences in processes associated with lymphocyte activation, immune effector functions, metabolic and signal transduction processes (Fig. 3A). Genes encoding inhibitory receptors (*Havrc2, Pdcd1*, *Ctla4*, and *Lag3*) and inflammation-associated cytokines like *Tnf* and *Il10* were upregulated in T cells from BDL mice, whereas transcription factors associated with effector T-cell functions, namely *Tbet*, *Tcf7*, *Eomes* and *Bcl6*,[12] were downregulated (Fig. 3B,C). P14 T cells from BDL mice showed increased expression of transcription factors associated with T-cell exhaustion, such as *Tox*, *Batf*, *Irf4* and *Id3*[13,14] (Fig. 3C). Further, gene set enrichment analysis (GSEA) for genes found in T-cell exhaustion in cancer and chronic viral infections[14] showed enrichment for these genes in P14 T cells from pLI mice (Fig. 3D,E). Flow cytometric analysis confirmed expression of these genes at the protein level in both transferred P14 (Fig. 3F) and endogenous LCMV-specific CD8 T cells in BDL mice (Fig. S3B,C). We further detected increased expression of PD1, TIM3 and LAG3 in virus-specific CD8 and CD4 T cells from the liver and spleen of both BDL and CCl_4-treated mice (Fig. S3D-F). To assess whether T-cell dysfunction in pLI coincided with expression of TOX, BATF and IRF4, we determined the expression of IFNg/TNF and these transcription factors in T cells on day 5 p.i., when precursors of exhausted T cells are known to emerge.[15] Although P14 T cells already lost their effector function by day 5 p.i. in BDL mice, no increased expression of TOX or BATF was detected at this time point (Fig. 3G). These results indicated that T-cell dysfunction during pLI was distinct from TOX-dependent exhausted T cells.

CD4 and CD8 T-cell dysfunction during liver injury is associated with IFN-I signaling

Chronic liver injury is associated with elevated expression of immune regulatory molecules,[1,16,17] which may curtail T cell-mediated immunity. GSEA revealed enrichment of 148 genes associated with TGFβ signaling in P14 T cells from BDL mice (Fig. 4A and Fig. S4A). Consistently, we detected increased levels of TGFβ expression in the liver (Fig. 4B) and enhanced levels of phospho-SMAD2 (Fig. 4C), a key downstream effector of TGFβ-receptor signaling in LCMV-specific CD8 T cells from BDL mice. To test the relevance of TGFβ-receptor signaling on T-cell dysfunction during pLI, we treated BDL mice with TGFβRII-blocking antibodies during LCMV infection. However, 60% of BDL mice succumbed after infection when TGFβ-receptor signaling was blocked (Fig. 4D), without evidence for increased viral clearance (Fig. 4E), suggesting a non-redundant and specific function of TGFβ in tissue-protection but not immune surveillance during liver injury.

Besides TGFβ, we also detected enhanced expression of IFN-I and the interferon-stimulated gene *Mx1* in livers of BDL mice that further increased after LCMV infection (Fig. 4F). GSEA indicated significant enrichment of 230 IFNAR signaling-associated genes[18] in P14 T cells from BDL mice (Fig. 4G, Fig. S4B). Among the top 20 upregulated genes, we found *Irf4*, *Nr4a2*, *Mt2*, *Egr2*, *Lclat1* and *Frmd4a* (Fig. 4H), which have been associated with T-cell dysfunction in cancer and chronic viral infections,[19] suggesting a potential role of IFN-I in T-cell dysfunction under pLI conditions. As reported before,[1] we found that translocation of gut microbiota in mice with BDL- and CCL_4-induced pLI- and patients with CLD (Fig. S4C,D) induced tonic IFNAR signaling in hepatic myeloid cells (Fig. S4E,F). Interestingly, colonization of BDL GF mice with the microbiome of sham-operated or BDL mice (Fig. S4G) led to comparable levels of IFN-I (Fig. S4H,I), suggesting that chronic IFNAR signaling during pLI was triggered by sensing translocated gut microbiota independent of its composition. More importantly, reduction of intestinal microbial burden by antibiotic treatment led to a reduction of IFN-I expression in the liver and intestine of BDL mice, improved expansion and effector cytokine production by LCMV-specific CD8 T cells and consequently enhanced viral clearance (Fig. S4J and Fig. 4I-K). These results demonstrated a critical role of microbial translocation in IFN-I production and T-cell dysfunction during chronic liver injury.

High IFN-I expression during pLI drives loss of T-cell immunity

Next, we investigated the relevance of IFN-I signaling for loss of T-cell immunity during liver injury. Antibody-mediated blockade of IFNAR in LCMV-infected pLI mice led to significant reduction of IFNAR-induced genes (Fig. S5A). Strikingly, inhibition of IFNAR signaling increased the numbers of total (Fig. S5B) and LCMV-specific CD8 and CD4 T cells in BDL as well as CCl_4-treated mice (Fig. 5A,C, Fig. S5B-H). Blockade of IFNAR signaling led to enhanced expression of IFNg/TNF in T cells and pronounced reduction of the viral load in pLI mice (Fig. S5A-E, Fig. S5D-H). Further we observed a reduction in PD1, TIM3 and LAG3 and TOX, IRF4 and BATF expression (Fig. S5F-I) in LCMV-specific CD8 T cells. Of note, IFNAR blockade induced higher numbers of $TCF1^+$P14 T cells and $TCF1^+TIM3^-$ progenitor exhausted cells (Fig. 5G,I). Thus, tonic IFNAR signaling in pLI mice determined T-cell dysfunction and viral persistence in a similar manner as in chronic LCMV infection with clone 13 and HIV infection.[10,20]

To explore the relevance of T cell-specific IFNAR signaling in their dysfunction during pLI, we generated CD4-Cre^{ERT2} *x* $IFNAR^{fl/fl}$ mice, in which tamoxifen injection deleted IFNAR selectively in ~60% of T cells (Fig. S6A). Tamoxifen application from day 3 after LCMV infection, neither restored T-cell function (Fig. S6B,C) nor improved viral clearance (Fig. S6D). Although this does not rule out a direct effect of IFN-I signaling on LCMV-specific CD8 T cells, it rather suggests a role of IFNAR signaling on other immune cell populations that then cause T-cell dysfunction. We therefore ablated IFNAR signaling in myeloid cells (*i.e.*, macrophages, monocytes and neutrophils), using LysM-Cre *x* $IFNAR^{fl/fl}$ mice. Strikingly, BDL LysM-Cre *x* $IFNAR^{fl/fl}$ mice showed a better control of LCVM infection compared to $IFNAR^{fl/fl}$ littermates ($Cre^{negative}$), had higher numbers of total and LCMV-specific CD8 T cells that produced more IFNg/TNF (Fig. 6A-G) and expressed lower levels of PD1, LAG3 and TIM3 (Fig. S6E,F). This suggests that IFNAR signaling in myeloid immune cells plays a key role in T-cell dysfunction during pLI. Furthermore, we detected elevated IL-10 levels in the blood of pLI mice after LCMV infection that were reduced by anti-IFNAR or antibiotic treatment (Fig. 6H). Likewise, we observed higher levels of phosphorylated-STAT3, the canonical downstream

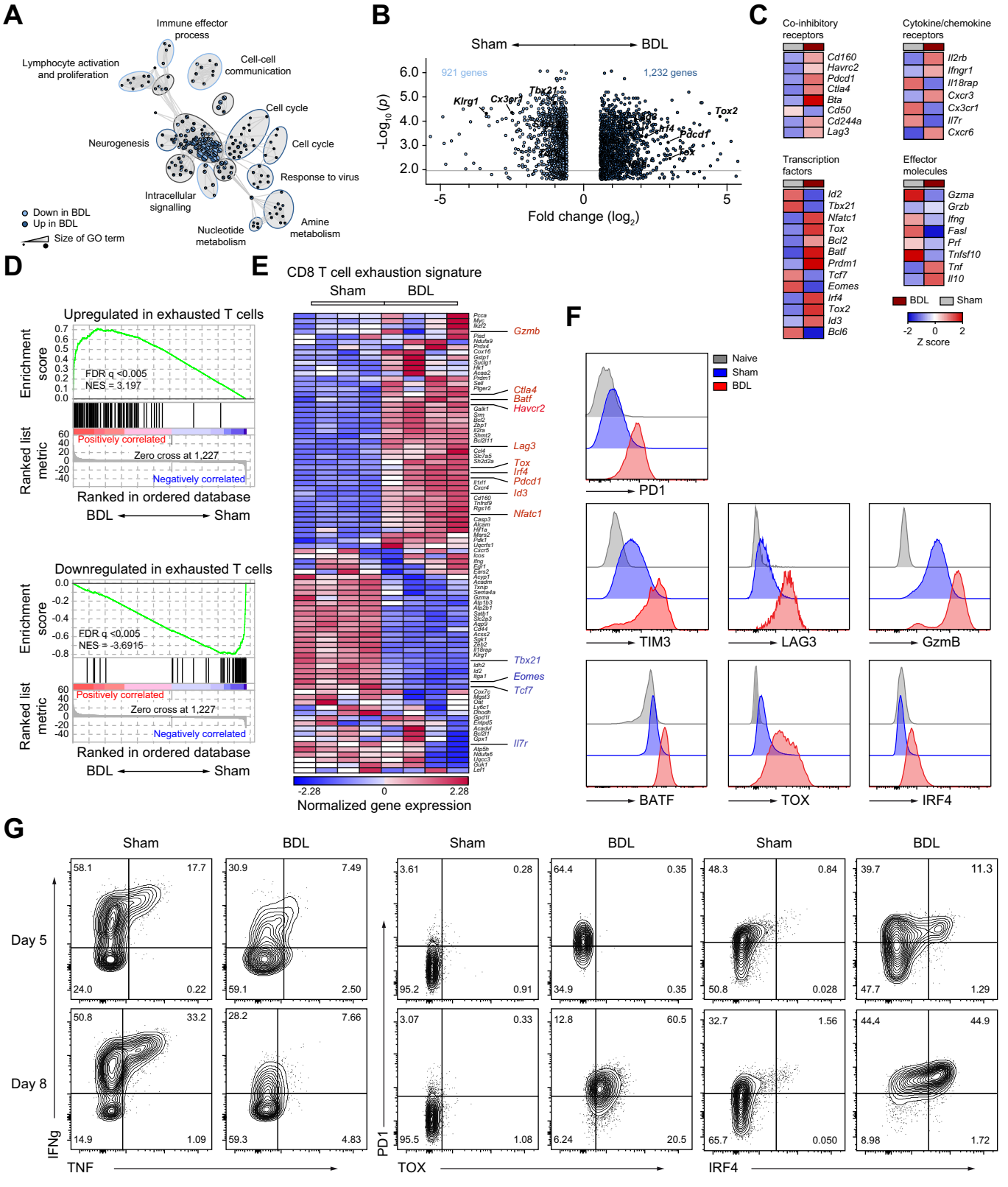

Fig. 3. T-cell exhaustion signature in antigen-specific T cells during pLI. (A-C) Gene-enrichment network (A), volcano plot (B) heatmap of centered mean expression (C) of DE genes in P14 T cells on day 8. (D) GSEA for exhausted T cell-associated genes. (E) Heatmap for DE genes in P14 T cells. (F,G) expression of inhibitory receptors and transcription factors in P14 T cells. (G) IFNg/TNF production, inhibitory receptors and transcription factor expression on day 5 or day 8. (F,G) Data representative of two independent experiments. DE, differntially expressed; GSEA, gene set enrichment analysis.

signaling molecule of IL-10R, upon anti-IFNAR treatment (Fig. 6I). GSEA showed enrichment of IL-10R-stimulated genes in P14 T cells from BDL mice (Fig. 6J), indicating a role for IFNAR-induced IL-10 in T-cell dysfunction during pLI. To prove this hypothesis, we generated MX1-Cre *x* IL-10 $^{fl/fl}$ mice, in which *Il10* gene is deleted upon expression of the IFNAR-stimulated gene MX1.[1] LCMV-specific CD8 and CD4 T-cell numbers were higher in BDL MX1-Cre *x* IL-10 $^{fl/fl}$ mice (Fig. 6K,L

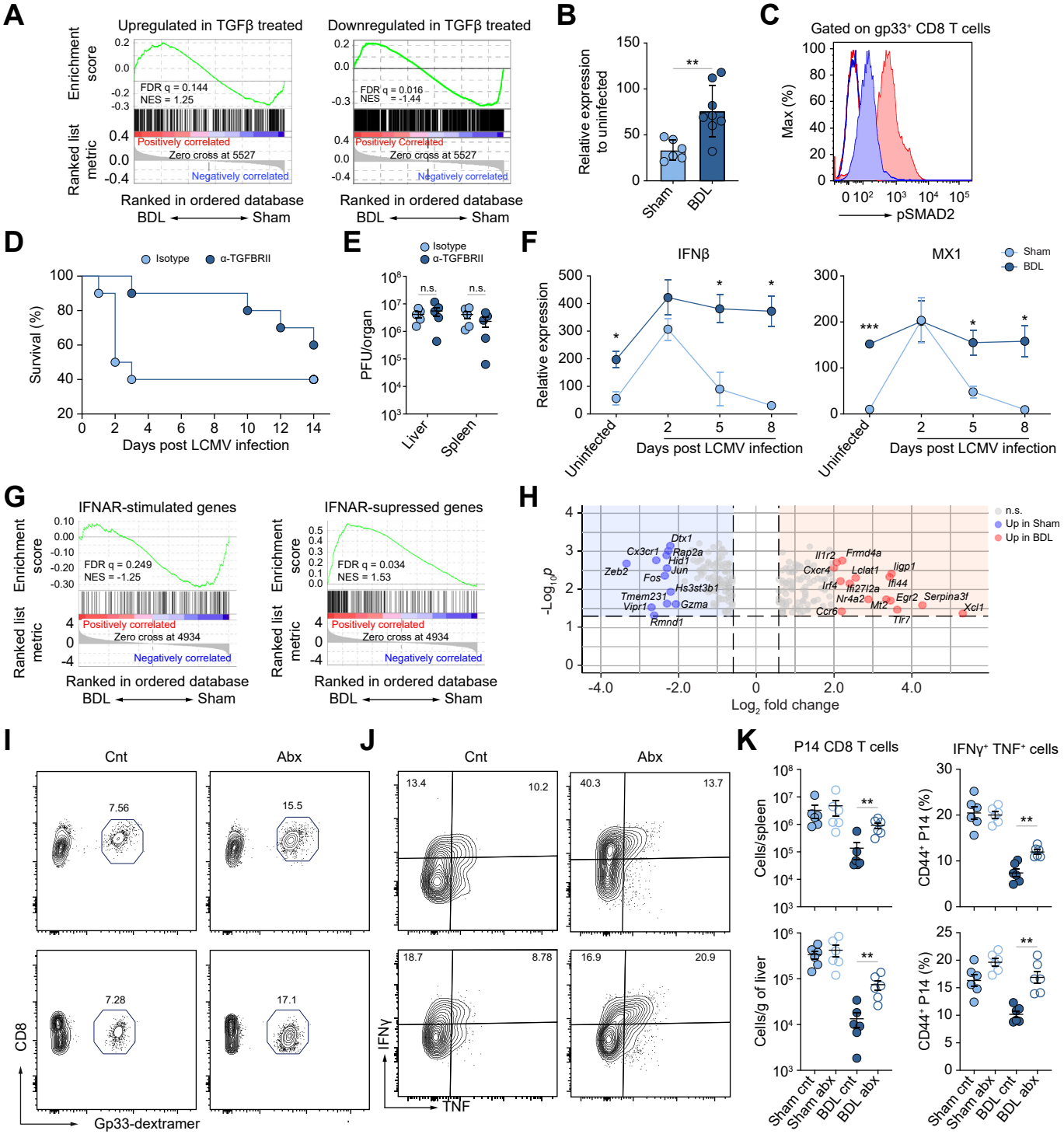

Fig. 4. Microbiota-induced IFN-I drives T-cell dysfunction during pLI. (A) GSEA of TGFβ-associated genes in P14 T cells on day 8 post infection. (B) Expression of *TGFβ* mRNA in the liver of mice in (A). (C) Phospho-Smad2 in LCMV-specific CD8 T cells. (D) Kaplan-Meier survival curves for LCMV-infected BDL mice receiving anti-TGFbR-II or isotype control. (E) Liver and spleen LCMV titers in mice in (D). (F) *IFNb* or *Mx1* mRNA expression in the liver. (G,H) GSEA (G) and volcano plot (H) of IFNAR-associated genes in P14 T cells. (I–K) Numbers and frequency of IFNg/TNF-producing P14 T cells in antibiotic (Abx)-treated BDL mice. (A) One-way ANOVA, (B–F,I–K) Data from ≥2 independent experiments. (B,E,F,K) Statistics were assessed by unpaired *t* test, (I,K) one-way ANOVA with Dunnett's multiple comparisons test. GSEA, gene set enrichment analysis; TGFbR-II, TGFb receptor II.

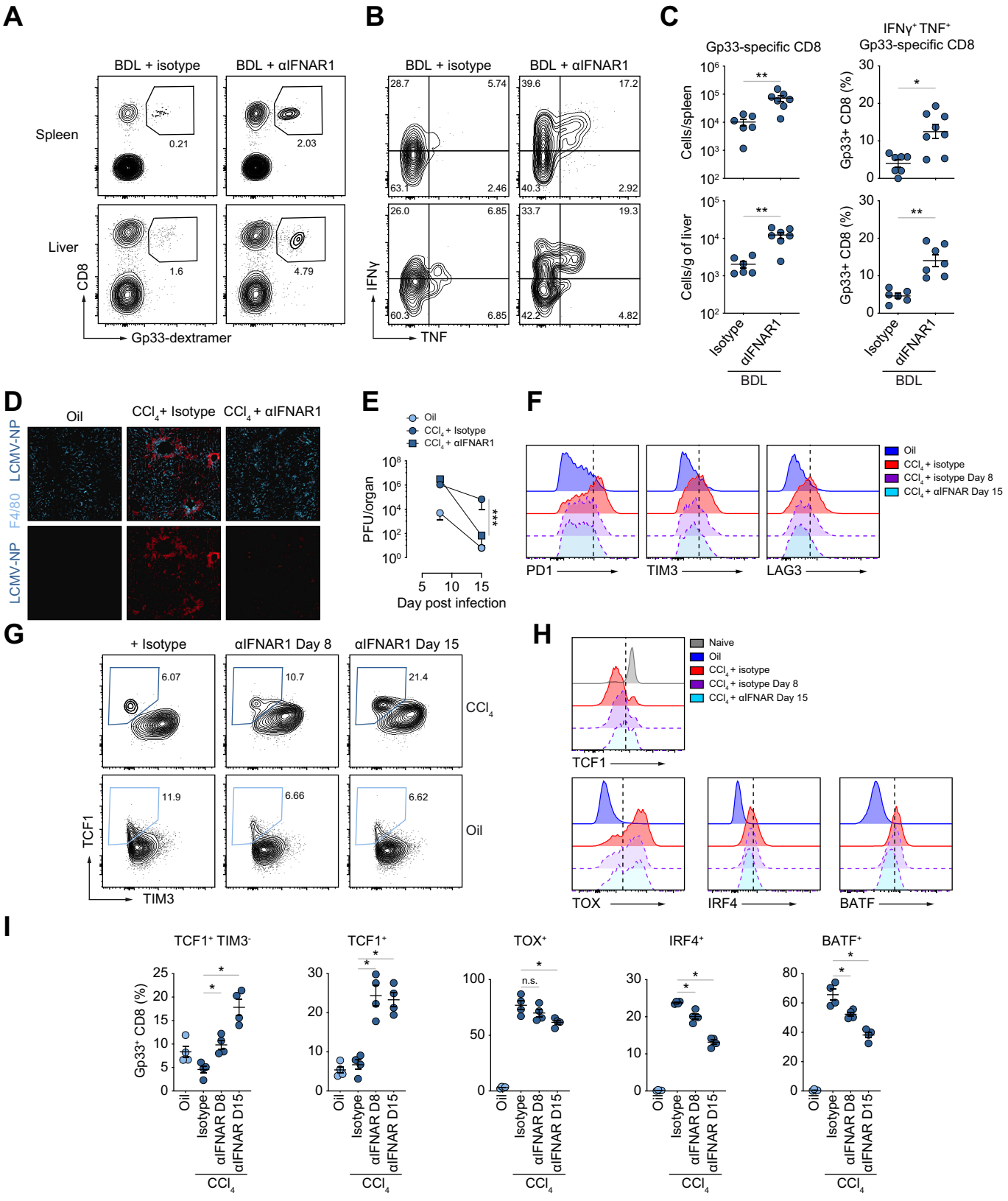

Fig. 5. Abrogation of IFNAR signaling improves LCMV-specific T-cell responses in pLI mice. pLI was induced by BDL or CCl_4 treatment before LCMV infection. Mice were treated with IFNAR1-blocking or isotype antibodies every second day starting at day 5 p.i. (A-C) Numbers of virus-specific and cytokine-producing LCMV-specific CD8 T cells on day 8 (A) and day 15 (B). (D) Liver immunofluorescence on day 15. (E) Quantification of LCMV titers in mice from (E). (F) expression of inhibitory receptors on LCMV-specific $CD8^+$ T cells. (G-I) Co-expression of the indicated marker in LCMV-specific CD8 T cells on day 15.(C,E,I) Statistics assessed by unpaired *t* test. BDL, bile duct ligation; CCl_4, carbone tetrachloride.

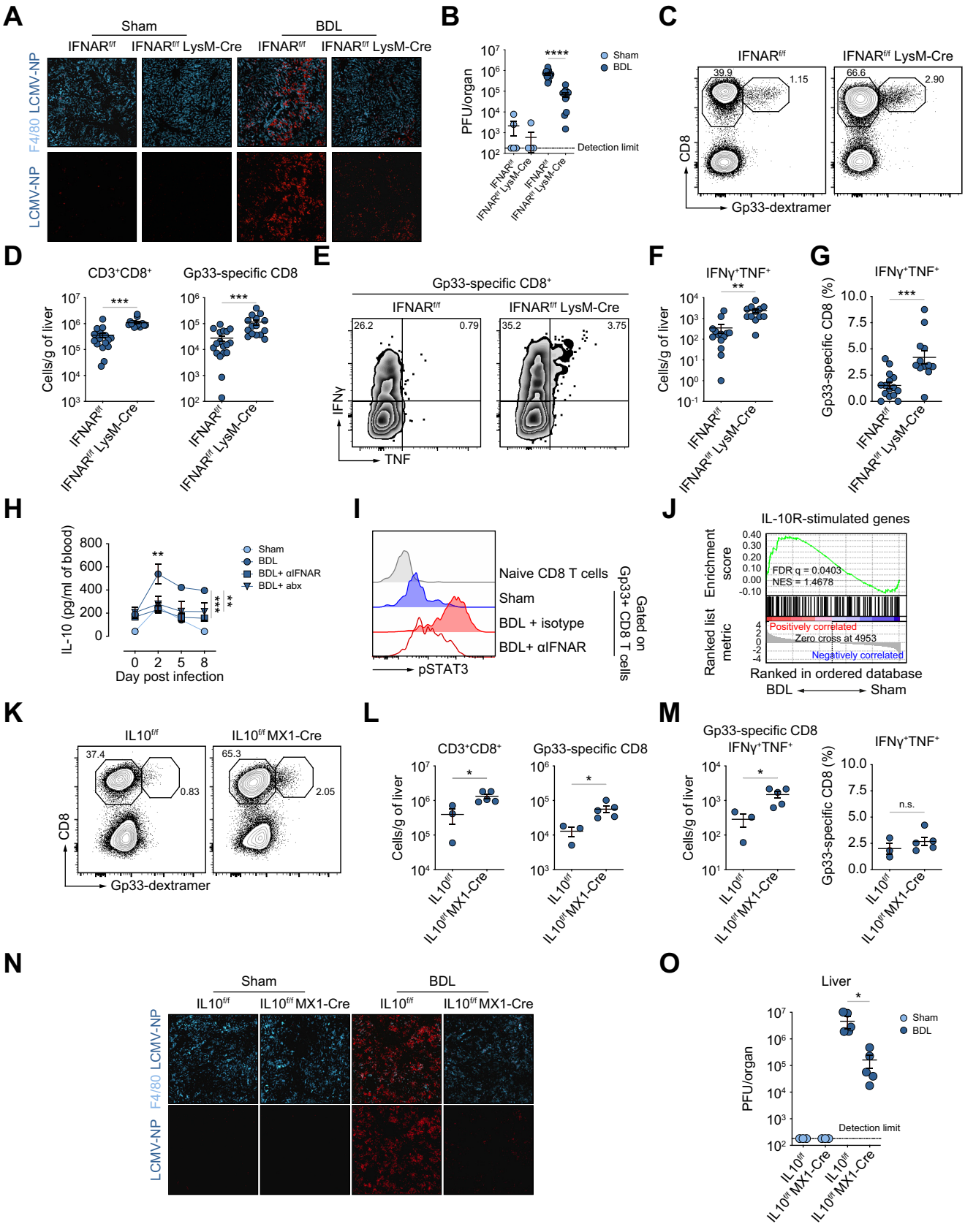
A
Sham
BDL
IFNAR f/f
IFNAR f/f LysM-Cre
F4/80 LCMV-NP
LCMV-NP
B
PFU/organ
Sham
BDL
Detection limit
C
IFNAR f/f
IFNAR f/f LysM-Cre
CD8
Gp33-dextramer
39.9
1.15
66.6
2.90
D
CD3+CD8+
Gp33-specific CD8
Cells/g of liver
E
Gp33-specific CD8+
IFNγ
TNF
26.2
0.79
35.2
3.75
F
IFNγ+TNF+
G
Gp33-specific CD8 (%)
H
IL-10 (pg/ml of blood)
Day post infection
BDL+ αIFNAR
BDL+ abx
I
Naive CD8 T cells
Sham
BDL + isotype
BDL+ αIFNAR
Gated on Gp33+ CD8 T cells
pSTAT3
J
IL-10R-stimulated genes
Enrichment score
FDR q = 0.0403
NES = 1.4678
Ranked list metric
Positively correlated
Zero cross at 4953
Negatively correlated
Ranked in ordered database
BDL
Sham
K
IL10 f/f
IL10 f/f MX1-Cre
37.4
0.83
65.3
2.05
L
M
n.s.
N
O
Liver

and Fig. S6G,H), with higher levels of IFNg/TNF production (Fig. 6M, Fig. S6I,J) and a reduced viral load (Fig. 6N,O) compared to littermate control mice. Overall, these data strongly indicate that IFNAR-induced IL-10 expression in myeloid cells contributed to T-cell dysfunction and failure to control viral infection during BDL- and CCL_4-induced pLI.

IL-10 acts directly on antigen-specific T cells during liver injury

To identify cell types on which IL-10 exerts its inhibitory effect, we determined IL-10Ra expression in different immune cell populations. While antigen-experienced ($CD44^+$) CD8, CD4 and LCMV-specific T cells in BDL mice expressed higher IL-10Ra levels (Fig. 7A,B, Fig. S7A), no changes in IL-10Ra expression were observed in myeloid immune cells or $CD44^-$ T cells (Fig. S7B-D). Importantly, we also detected elevated surface expression levels of IL-10Ra on $CD45RA^{neg}$ T cells in patients with cirrhosis compared to healthy individuals (Fig. 7C), suggesting a higher sensitivity to IL-10 signaling in activated T cells during pLI. To assess the relevance of IFNAR signaling, we treated murine T cells with IFN-I for 48 h before T-cell receptor stimulation *in vitro* or induced IFN-I production *in vivo* by administering polyI:C for 1-3 days. Pre-exposure of T cells to IFN-I upregulated IL-10Ra expression in a time- and dose-dependent manner (Fig. 7D,E).

To investigate whether IL-10 was acting directly on T cells, we co-transferred equal numbers of WT ($CD45.2^+$) or CD4-dominant-negative IL-10Ra TG ($CD45.1/2^+$) T cells, which overexpressed a dominant-negative IL-10Ra and therefore had impaired IL-10 signaling,[21] into irradiated WT mice. After induction of liver injury, chimeric mice (Fig. S7E) were infected with LCMV and T cells were analyzed on day 8 p.i. Strikingly, total numbers of activated TG CD8 T cells in the liver were significantly higher compared to WT cells (Fig. 7F). More importantly, CD4 and CD8 T cells with impaired IL-10Ra signaling were more prevalent among LCMV-specific T cells and had superior effector cytokine production compared to WT cells (Fig. 7G,H). Consistently, mice that received IL-10Ra-impaired T cells showed significantly lower viral load compared to their counterparts that received WT T cells (Fig. 7I). Thus, T cells with low responsiveness to IL-10 showed an improved proliferative capacity and effector cytokine production during pLI. Of note, TG LCMV-specific T cells had lower expression levels of PD-1, LAG-3 or TIM3 but no differences in expression of IRF4, TOX or BATF (Fig. 7J, Fig. S7F). Collectively, these results suggested that elevated levels of IL-10 during liver injury were responsible for T-cell dysfunction and impaired viral clearance.

Therapeutic targeting and inhibition of IL-10 signaling restores T-cell responses during liver injury

Next, we investigated whether therapeutic interference with IL-10R downstream signaling restores antiviral T-cell immune surveillance during liver injury. Efficient IL-10Ra blockade, as indicated by reduced pSTAT3 expression (Fig. S8A), in LCMV-infected BDL and CCL_4-treated mice led to increased numbers of LCMV-specific CD8 T cells with higher IFNg/TNF production and reduced PD-1, LAG-3 and TIM3 expression (Fig. 8A-D, Fig. S8B-E). Consistently, IL-10Ra blockade reconstituted clearance of viral infection in BDL and CCl_4-treated mice similar to healthy mice by day 15 p.i. (Fig. 8E-G). Moreover, IL-10Ra blockade enhanced the frequencies of $TCF1^+TIM3^{neg}$ T cells (Fig. S8F) and reduced TOX, IRF4 and BATF expression (Fig. 8H,I). Likewise, we observed a significant increase in the frequency of HBs-specific CD8 T cells, as well IFNg/TNF CD8 T cells in HBs-vaccinated pLI mice upon treatment with anti-IL-10R antibodies (Fig. S8G,H). Next, we wondered whether interference with IL-10Ra signaling would also restore dysfunctional T cells from patients with CLD. Antibody-mediated blockade of the IL-10Ra in αCD3/CD28-stimulated T cells from patients with cirrhosis reduced PD-1 and CTLA-4 expression (Fig. 8J and Fig. S8I). More importantly, IL-10Ra blockade enhanced the proliferation, as well as IL-21 and IFNg production (Fig. 8K,L, Fig. S8J,K), of T cells from vaccinated patients with cirrhosis upon stimulation with HBs peptides. Together, these data revealed that therapeutic blockade of IL-10Ra-signaling restored T-cell immune surveillance during BDL- and CCL_4-induced pLI in mice and in patients with cirrhosis.

Discussion

CAID is linked to poor responses to vaccination and occurrence of infections that can cause loss-of-function of remaining liver tissue and thereby trigger life-threatening liver failure,[7,22–24] against which no specific therapeutic intervention exists. While intractable bacterial infections pose the most prominent threat to patients with cirrhosis,[23] viral infections also cause liver failure and difficult-to-treat infections in these patients.[25,26] Herein, we identified the IFN-I/IL-10 signaling axis as a determinant of CAID, through which liver damage is linked to suppression of systemic T-cell immunity in response to acute LCMV infection in preclinical models of pLI and to vaccination in pLI mice and patients with cirrhosis.

The outcome of immunity to viral infection is determined by both virus-intrinsic properties and host factors. Virus-intrinsic properties and their contribution to the development of persistent viral infection have been extensively studied, such as LMCV clone 13 infection overcoming antiviral immunity by inducing T-cell exhaustion,[13–15] HIV achieving persistence through viral integration into the host genome of T cells,[26] or HBV establishing robust viral latency in hepatocytes and exploiting the liver's tolerogenic properties.[27,28] On the other side, host factors[7,29,30] such as age, inflammation and comorbidities, amongst which antiviral immune responses develop, also shape the outcome of infection.[31] In patients with COVID-19 and cardiovascular, lung or metabolic diseases, overshooting immune responses that cause organ pathology

Fig. 6. Abrogation of IFNAR/IL-10 axis restores T-cell immunity in pLI. (A-G) $IFNAR^{flox/flox}$ and $IFNAR^{flox/flox}$xLysm-Cre mice were infected with LCMV after BDL and analyzed on day 8. (A) Liver immunofluorescence for LCMV nucleoprotein and macrophages, (B) liver LCMV titers. (C,D) Quantification of virus-specific CD8 T cells and (E-G) cytokine-producing T cells. (H) IL-10 levels in blood of BDL mice treated with anti-IFNAR antibodies or antibiotic (Abx). (I) Phospho-STAT3 in LCMV-specific CD8 T cells at day 8 p.i. and after IFNAR-blockade. (J) GSEA of IL-10R-associated genes in LCMV-specific P14 T cells. (K–O) $IL10^{f/f}$ Mx1-Cre^+ or $IL10^{f/f}$ (Cre-) littermates were infected with LCMV after the BDL operation. (K-M) Frequencies and numbers of hepatic $CD8^+$ T cells, LCMV-specific CD8 T cells and IFNg/TNF-producing LCMV-specific CD8 T cells. (M) Liver immunofluorescence of LCMV nucleoprotein and macrophages.(O) Liver LCMV titers. Data obtained from three (A-G), or two (K–O) independent experiments. (B,D,F,G,J,N,O) Statistics assessed by unpaired *t* test, (H) one-way ANOVA with Dunnett's multiple comparisons test. BDL, bile duct ligation.

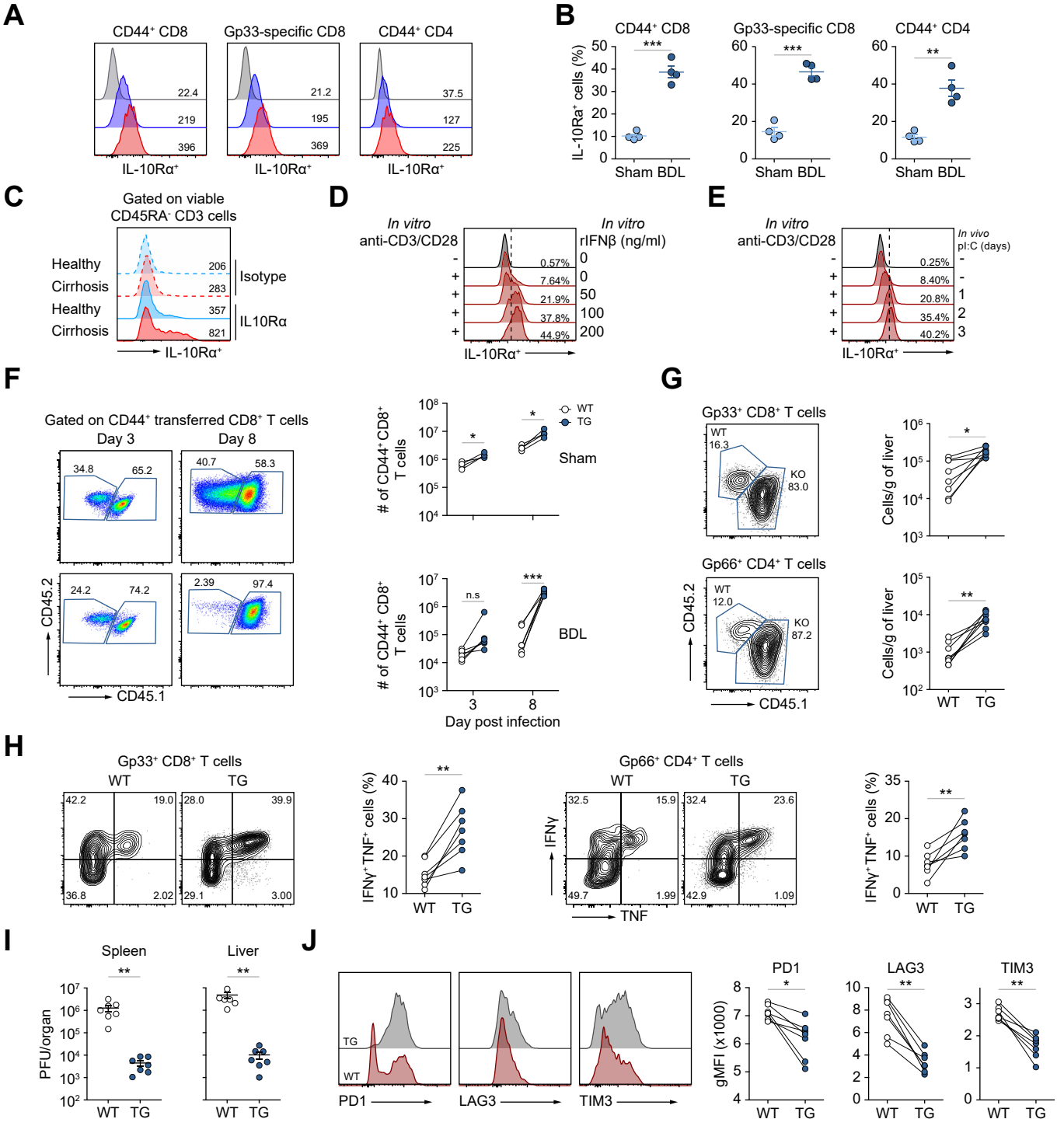

Fig. 7. T-cell-specific IL-10Ra-signaling hampers anti-LCMV immune responses. (A,B) Expression level and percentage of IL-10Ra-expressing T cells from BDL- or sham-operated mice at day 8. (C) IL10Ra expression on peripheral blood $CD3^{+}CD45RA^{neg}$ T cells of healthy donors or patients with cirrhosis. (D) IL10Ra expression of murine T cells stimulated *ex vivo* with αCD3/CD28 in the presence of increasing IFNβ concentrations. (E) IL10Ra expression after *ex vivo* stimulation with αCD3/CD28 in murine T cells isolated 3 days after pI:C application. (F–K) Sub-lethally irradiated B6 mice (CD45.1) received 1:1 mixture of naïve WT ($CD45.2^{+}$) and TG ($CD45.1/2^{+}$) T cells. 4 weeks later mice underwent sham operation or BDL and were infected with LCMV. (F–H) Abundance of TG and WT CD8 T cells, (F) LCMV-specific CD8 T cells or LCMV-specific CD4 T cells, (G) IFNg/TNF production in LCMV-specific T cells (H). (I) Liver and spleen LCMV-titer in BDL mice receiving either WT or TG T cells. (J) Expression of inhibitory receptors in LCMV-specific CD8 T cells. Data from three independent experiments (A-J) and (C) with individual donors. (B,I) Statistics assessed by unpaired *t* tests, and (F-J) two-tailed paired Student's *t* test. BDL, bile duct ligation; TG, transgenic; WT, wild type.

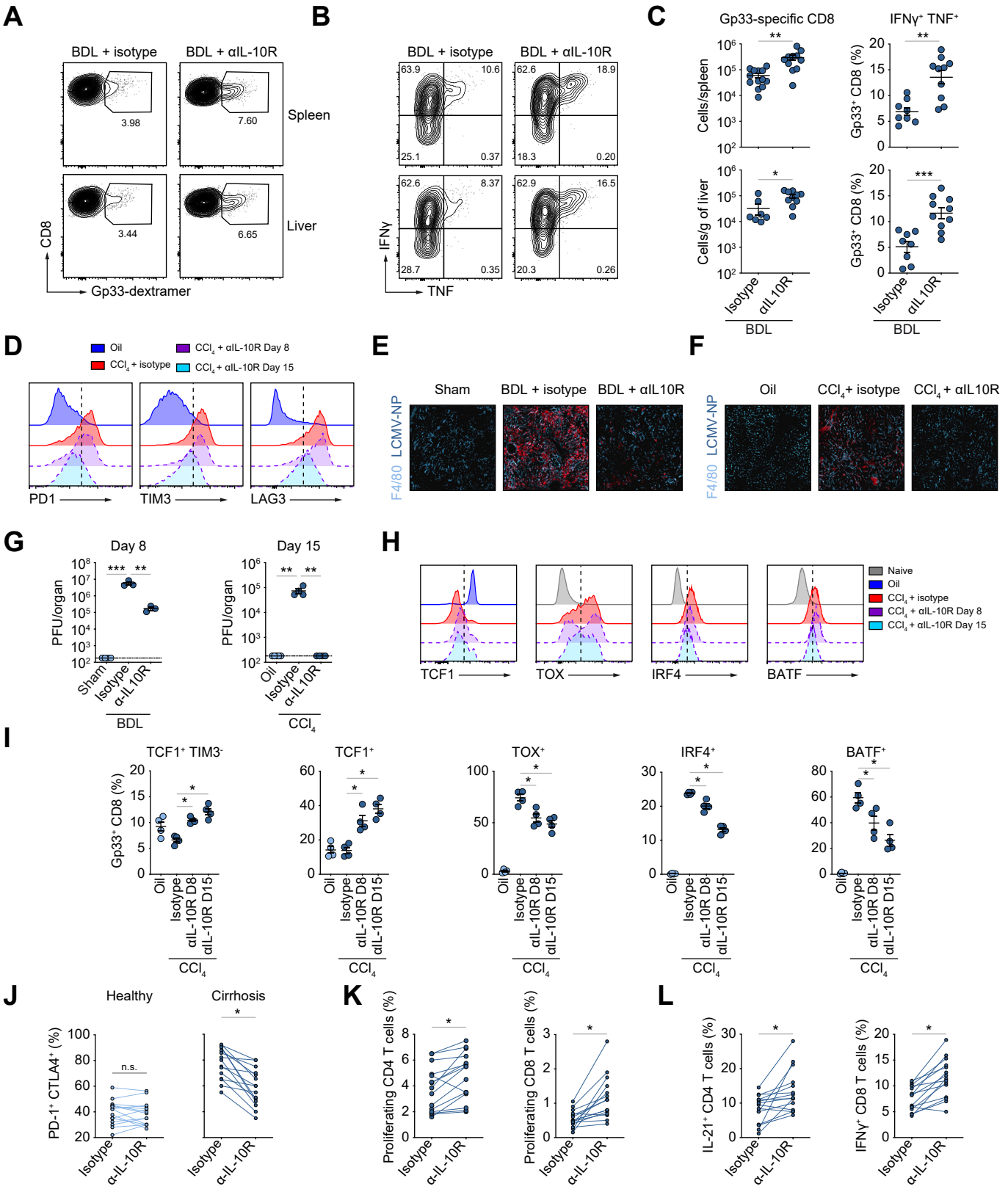

Fig. 8. IL-10Ra blockade restores T-cell immunity during pLI. BDL- or CCl_4-treated mice received anti-IL-10Ra antibody every second day during LCMV infection. (A-C) Frequencies and numbers of LCMV-specific and IFNg/TNF-producing T cells. (D) Expression of inhibitory receptors by LCMV-specific CD8 T cells (D). (E-G) Liver immunofluorescence and liver LCMV titers. (H,I) Expression of indicated marker in LCMV-specific CD8 T cells. (J) Co-expression of PD1 and CTLA4 in CD8 T cells from PBMCs of healthy controls or patients with cirrhosis after stimulation with anti-CD3/CD28 in the presence of anti-IL10Ra or isotype control. (K,L) T cells from HBsAg-vaccinated healthy controls (n = 4) and patients with cirrhosis (n = 4) stimulated with HBsAg peptides in the presence of anti-IL10Ra or isotype control. (K) Frequencies of proliferating, (l) cytokine-producing CD4 and CD8 T cells. (A-G) Data from three independent experiments and (J-L) one experiment with individual donors. (C,G,I)

Statistics assessed by unpaired *t* tests. (J-L) two-tailed paired Student's *t* test. n.s., not significant, *$p \leq 0.05$, **$p \leq 0.01$, ***$p \leq 0.001$, ****$p \leq 0.0001$. HBsAg, hepatitis B virus surface antigen.

are more frequently observed.[25,32] However, during CLD and cirrhosis patients suffer from an attenuated and dysfunctional immune response, largely driven by loss of tissue architecture and systemic chronic inflammation.[7,24]

The liver serves as a firewall that eliminates intestinal microbiota that have gained access to portal venous blood.[33] In patients with CLD, increased microbial translocation is believed to cause systemic inflammation.[34,35] Our results demonstrated that enhanced microbial translocation after liver injury caused increased tonic IFNAR signaling in liver myeloid cells and that abrogation of IFNAR signaling in these cells prevented loss of systemic T-cell immunity. It is well established that intestinal microbiota play a key role in the pathology and progression of liver diseases.[36,37] Interestingly, reconstitution of GF mice with gut microbiota from either healthy mice or mice with liver injury led to similar levels of IFN-I and similar loss of systemic T-cell immunity. This suggests that IFNAR-induced loss of systemic T-cell immunity during pLI is rather driven by the innate sensing of translocated gut bacteria, and raised the question of how IFN signaling in myeloid cells might regulate T-cell function.

Genome-wide transcriptional and protein profiling of LCMV-specific T cells from pLI mice revealed gene signatures characteristic of exhausted T cells found in cancer or chronic infection. However, loss of T-cell effector function in pLI mice preceded the upregulation of exhaustion-associated transcription factors; TOX, BATF and IRF4, corroborating our assumption that loss of T-cell immunity during liver injury is not a cell-intrinsic process but is driven in a paracrine fashion. Of note, we detected gene signatures for TGFβ, IFN and IL-10 signaling among others. It was previously shown that blockade of TGFβ signaling does not lead to control of persistent viral infection under healthy conditions.[38] Our experiments confirmed these findings in the context of pLI and revealed a non-redundant role of TGFβ in organ protection during pLI as its blockade led to severe liver immune pathology. Importantly, after LCMV infection of mice with liver injury we detected increased IL-10 expression in monocytes/macrophages that depended on IFN-I signaling, which is unexpected because IFN-I is considered to be involved in self-perpetuating inflammation.[39] In contrast to the immune pathology-promoting effect of blocking TGFβ, inhibition of IL-10 by antibodies or T cell-specific ablation of IL-10R signaling rescued effector function of LCMV-specific T cells in pLI mice and promoted viral clearance in the absence of notable immune pathology. Likewise, elimination of intestinal microbiota and reducing gut microbial translocation to the liver and blockade of IFN-I signaling in myeloid cells all prevented the excessive production of IL-10 and rescued antiviral T-cell function. Translating these results from preclinical models of liver injury to patients with CLD, our data suggest that inhibition of IL-10R signaling rescued vaccination-induced antigen-specific T cells from their dysfunction.

Although our data provides *in vitro*, *in vivo* and human evidence of this particular mechanism, the study may still have some limitations. First, none of the current mouse models faithfully reflect all etiological and pathophysiological characteristics of chronic liver disease and cirrhosis in humans. The BDL and CCl_4 models used in this study mainly induce prolonged liver injury, which indeed recapitulates several relevant aspects and complications observed in patients with cirrhosis, namely microbial translocation, chronic IFNAR signaling and immune dysfunction. It remains unclear whether acute liver injury or changes in the liver architecture occurring in cirrhosis patients further contribute to the mechanisms described here, such as enhanced gut bacterial translocation, or whether cirrhosis-associated ultrastructural changes themselves may influence hepatic or systemic immunity. Second, IL-10 signaling is a key regulator of immune effector functions and tissue integrity,[40] and its blockade may therefore carry the risk of inducing immunopathology or autoimmunity. Therefore, future studies aiming at overcoming the limitations of IL-10 signaling in CAID will need to fine-tune the duration, timing and levels of IL-10 inhibition before this approach can be used to increase vaccination efficacy in patients with CLD.

Taken together, our work provides a mechanistic understanding of the loss of systemic T-cell immunity during chronic liver injury, discriminates organ-protective TGFβ-signaling from T-cell suppressing IL-10 signaling and identifies IFN-I and IL-10 as molecular targets for immune interventions that reconstitute T-cell immunity.

Affiliations

[1]Institute of Molecular Medicine and Experimental Immunology, University Hospital Bonn, Germany; [2]Institute of Innate Immunity, University Hospital Bonn, Germany; [3]Medizinische Klinik und Poliklinik, Hamburg Center for Translational Immunology (HCTI), Universitätsklinikum Hamburg-Eppendorf, 20246 Hamburg, Germany; [4]Medizinische Klinik 1. Universitätsklinikum Frankfurt. Goethe Universität I. Medizinische Klinik und Poliklinik, Germany; [5]Molecular Immunology in Neurodegeneration, German Center for Neurodegenerative Diseases (DZNE), Bonn, Germany; [6]Institute for Hygiene and Public Health, University Hospital Bonn, Germany; [7]Department of Immunobiology, Yale University School of Medicine, New Haven, CT, USA; [8]Institute of Virology, University Hospital Bonn, Germany; [9]German Center for Infection Research, Bonn-Cologne site; [10]Institute of Immunology, University of Heidelberg, Germany; [11]Institute of Molecular Immunology and Experimental Oncology, Technical University of Munich, Germany; [12]current address: Peter Medawar Building for Pathogen Research, Nuffield Department of Medicine, University of Oxford, UK; [13]German Center for Infection Research, Munich site.

Abbreviations

BDL, bile duct ligation/bile duct ligated; CAID, cirrhosis-associated immune dysfunction; CCl_4, carbon tetrachloride; CLD, chronic liver disease; GSEA, gene set-enrichment analysis; IFN, interferon; IFNRA, type I interferon receptors; IL-10, interleukin-10; LCMV, lymphocytic choriomeningitis virus; PBMCs, peripheral blood mononuclear cells; PFUs, plaque-forming units; pLI, prolonged liver injury; TG, transgenic; WT, wild-type.

Financial support

ZA, PAK, SVS were supported by the German Research Foundation (DFG) projects: Excellence Cluster EXC 2151 (ID: 390873048). ZA, PAK were supported by SFBTR57 ((2)-P32 and -P11) (ID: 36842431). ZA, was supported by the GRK 2168 (ID: 272482170), SFB1454 (P10) (ID: 432325352), SFBTR237 (B15) (ID: 369799452), and by the German Federal Ministry of Education and Research (BMBF) for the COVIMMUNE project. CPH was supported by the DFG (project

number 403193363) and the Wellcome Trust (WT109965MA). PAK was supported by the European Union's Horizon 2020 research and innovation programme TherVacB, by the SFB-TRR179 and the German Center for Infection Research, Munich site. The DFG funded equipment used for flow cytometry (project numbers 21637201, 471514137, 387333827, and 216372545).

Conflict of interest

The authors declare that they have no conflict of interest.

Please refer to the accompanying ICMJE disclosure forms for further details.

Authors' contributions

Acquisition of data (CPH, JS, LMA, HH, SVS, RS, SK, TB, JS, BMK, ZA, BS, NK); study concept and design (CPH, CK, JT, NG, BMK, AR, SVS, ZA, PAK); analysis and interpretation of data (CPH, JS, SVS, ZA, KS, NG, AR, EL, JT, PAK); drafting the manuscript (ZA, PAK, CPH, AR, SVS).

Data availability statement

All data from this study are provided in the source data. RNA-seq expression data are available at NCBI GEO under the accession number: GSE158261. Primary data from flow cytometry or immunohistochemistry are available upon reasonable request.

Acknowledgments

We thank Alisa Ismaili, Maike Kreutzenbeck, Janett Wieseler, Sven Kröcker and Rebecca Balduf for technical assistance. We thank Dr. Michael Brinkmann and Lisa Brinkmann for the excellent support of the vaccination studies. We would like to acknowledge the support by the Flow Cytometry and Next Generation Sequencing Core Facilities at the Medical Faculty at the University of Bonn. The DFG funded equipment used for flow cytometry (project numbers 21637201, 471514137, 387333827, and 216372545).

Supplementary data

Supplementary data to this article can be found online at https://doi.org/10.1016/j.jhep.2023.02.026.

References

Author names in bold designate shared co-first authorship

[1] **Hackstein CP**, **Assmus LM**, Welz M, Klein S, Schwandt T, Schultze J, et al. Gut microbial translocation corrupts myeloid cell function to control bacterial infection during liver cirrhosis. Gut 2017;66:507–518.
[2] Wiest R, Lawson M, Geuking M. Pathological bacterial translocation in liver cirrhosis. J Hepatol 2014;60:197–209.
[3] Albillos A, Lario M, Alvarez-Mon M. Cirrhosis-associated immune dysfunction: distinctive features and clinical relevance. J Hepatol 2014;61:1385–1396.
[4] Chou AL, Huang WW, Lin MN, Su CC. Human herpesvirus type 8 in patients with cirrhosis independent of thrombocytopenia. J Clin Pathol 2010;63:254–258.
[5] Premkumar M, Devurgowda D, Dudha S, Maiwall R, Bihari C, Grover S, et al. A/H1N1/09 influenza is associated with high mortality in liver cirrhosis. J Clin Exp Hepatol 2019;9:162–170.
[6] Schutte A, Ciesek S, Wedemeyer H, Lange CM. Influenza virus infection as precipitating event of acute-on-chronic liver failure. J Hepatol 2019;70:797–799.
[7] Albillos A, Martin-Mateos R, Van der Merwe S, Wiest R, Jalan R, Álvarez-Mon M. Cirrhosis-associated immune dysfunction. Nat Rev Gastroenterol Hepatol 2022;19:112–134.
[8] Alter MJ. Vaccinating patients with chronic liver disease. Gastroenterol Hepatol (N Y) 2012;8:120–122.
[9] Arvaniti V, D'Amico G, Fede G, Manousou P, Tsochatzis E, Pleguezuelo M, et al. Infections in patients with cirrhosis increase mortality four-fold and should be used in determining prognosis. Gastroenterology 2010;139:1246–1256. 1256 e1241-1245.
[10] Zhen A, Rezek V, Youn C, Lam B, Chang N, Rick J, et al. Targeting type I interferon-mediated activation restores immune function in chronic HIV infection. J Clin Invest 2017;127:260–268.
[11] Roni DA, Pathapati RM, Kumar AS, Nihal L, Sridhar K, Tumkur Rajashekar S. Safety and efficacy of hepatitis B vaccination in cirrhosis of liver. Adv Virol 2013;2013:196704.
[12] Intlekofer AM, Takemoto N, Wherry EJ, Longworth SA, Northrup JT, Palanivel VR, et al. Effector and memory CD8+ T cell fate coupled by T-bet and eomesodermin. Nat Immunol 2005;6:1236–1244.
[13] Khan O, Giles JR, McDonald S, Manne S, Ngiow SF, Patel KP, et al. TOX transcriptionally and epigenetically programs CD8(+) T cell exhaustion. Nature 2019;571:211–218.
[14] **Man K**, **Gabriel SS**, Liao Y, Gloury R, Preston S, Henstridge DC, et al. Transcription factor IRF4 promotes CD8(+) T cell exhaustion and limits the development of memory-like T cells during chronic infection. Immunity 2017;47:1129–1141 e1125.
[15] **Utzschneider DT**, **Gabriel SS**, Chisanga D, Gloury R, Gubser PM, Vasanthakumar A, et al. Early precursor T cells establish and propagate T cell exhaustion in chronic infection. Nat Immunol 2020;21:1256–1266.
[16] **Beyer M**, **Abdullah Z**, **Chemnitz JM**, Maisel D, Sander J, Lehmann C, et al. Tumor-necrosis factor impairs CD4(+) T cell-mediated immunological control in chronic viral infection. Nat Immunol 2016;17:593–603.
[17] Seki E, De Minicis S, Osterreicher CH, Kluwe J, Osawa Y, Brenner DA, et al. TLR4 enhances TGF-beta signaling and hepatic fibrosis. Nat Med 2007;13:1324–1332.
[18] Rusinova I, Forster S, Yu S, Kannan A, Masse M, Cumming H, et al. Interferome v2.0: an updated database of annotated interferon-regulated genes. Nucleic Acids Res 2013;41:D1040–D1046.
[19] Williams MA, Bevan MJ. Immunology: exhausted T cells perk up. Nature 2006;439:669–670.
[20] Teijaro JR, Ng C, Lee AM, Sullivan BM, Sheehan KC, Welch M, et al. Persistent LCMV infection is controlled by blockade of type I interferon signaling. Science 2013;340:207–211.
[21] **Kamanaka M**, **Huber S**, **Zenewicz LA**, Gagliani N, Rathinam C, O'Connor Jr W, et al. Memory/effector (CD45RB(lo)) CD4 T cells are controlled directly by IL-10 and cause IL-22-dependent intestinal pathology. J Exp Med 2011;208:1027–1040.
[22] Arroyo V, Moreau R, Kamath PS, Jalan R, Ginès P, Nevens F, et al. Acute-on-chronic liver failure in cirrhosis. Nat Rev Dis Primers 2016;2:16041.
[23] Moreau R, Jalan R, Gines P, Pavesi M, Angeli P, Cordoba J, et al. Acute-on-chronic liver failure is a distinct syndrome that develops in patients with acute decompensation of cirrhosis. Gastroenterology 2013;144:1426–1437. 1437.e1421-e1429.
[24] Hasa E, Hartmann P, Schnabl B. Liver cirrhosis and immune dysfunction. Int Immunol 2022;34:455–466.
[25] Brodin P. Immune determinants of COVID-19 disease presentation and severity. Nat Med 2021;27:28–33.
[26] Cohn Lillian B, Silva Israel T, Oliveira Thiago Y, Rosales Rafael A, Parrish Erica H, Learn Gerald H, et al. HIV-1 integration landscape during latent and active infection. Cell 2015;160:420–432.
[27] **Limmer A**, **Ohl J**, Kurts C, Ljunggren HG, Reiss Y, Groettrup M, et al. Efficient presentation of exogenous antigen by liver endothelial cells to CD8+ T cells results in antigen-specific T-cell tolerance. Nat Med 2000;6:1348–1354.
[28] Protzer U, Maini MK, Knolle PA. Living in the liver: hepatic infections. Nat Rev Immunol 2012;12:201–213.
[29] Lebosse F, Gudd C, Tunc E, Singanayagam A, Nathwani R, Triantafyllou E, et al. CD8(+)T cells from patients with cirrhosis display a phenotype that may contribute to cirrhosis-associated immune dysfunction. EBioMedicine 2019;49:258–268.
[30] Wasmuth HE, Kunz D, Yagmur E, Timmer-Stranghoner A, Vidacek D, Siewert E, et al. Patients with acute on chronic liver failure display "sepsis-like" immune paralysis. J Hepatol 2005;42:195–201.
[31] Virgin HW, Wherry EJ, Ahmed R. Redefining chronic viral infection. Cell 2009;138:30–50.
[32] Cao X. COVID-19: immunopathology and its implications for therapy. Nat Rev Immunol 2020;20:269–270.
[33] Balmer ML, Slack E, de Gottardi A, Lawson MA, Hapfelmeier S, Miele L, et al. The liver may act as a firewall mediating mutualism between the host and its gut commensal microbiota. Sci Transl Med 2014;6:237ra266.
[34] Hartmann P, Chu H, Duan Y, Schnabl B. Gut microbiota in liver disease: too much is harmful, nothing at all is not helpful either. Am J Physiol Gastrointest Liver Physiol 2019;316:G563–G573.
[35] Trebicka J, Macnaughtan J, Schnabl B, Shawcross DL, Bajaj JS. The microbiota in cirrhosis and its role in hepatic decompensation. J Hepatol 2021;75(Suppl 1):S67–S81.
[36] Wang R, Tang R, Li B, Ma X, Schnabl B, Tilg H. Gut microbiome, liver immunology, and liver diseases. Cell Mol Immunol 2021;18:4–17.

[37] Trebicka J, Bork P, Krag A, Arumugam M. Utilizing the gut microbiome in decompensated cirrhosis and acute-on-chronic liver failure. Nat Rev Gastroenterol Hepatol 2021;18:167–180.
[38] Boettler T, Cheng Y, Ehrhardt K, von Herrath M. TGF-beta blockade does not improve control of an established persistent viral infection. Viral Immunol 2012;25:232–238.
[39] Crow YJ, Lebon P, Casanova JL, Gresser I. A brief historical perspective on the pathological consequences of excessive type I interferon exposure *in vivo*. J Clin Immunol 2018;38:694–698.
[40] O'Garra A, Barrat FJ, Castro AG, Vicari A, Hawrylowicz C. Strategies for use of IL-10 or its antagonists in human disease. Immunol Rev 2008;223:114–131.